

## PREDICTION OF BURST IN ALUMINUM TUBE HYDROFORMING USING NON-QUADRATIC YIELD FUNCTIONS

Y.P. Korkolis<sup>1</sup> and S. Kyriakides<sup>1</sup>

<sup>1</sup>Research Center for Mechanics of Solids, Structures & Materials  
The University of Texas at Austin  
e-mails: ikorko@mail.utexas.edu, skk@mail.utexas.edu,  
Web page: <http://www.ae.utexas.edu/research/mssm/>

### ABSTRACT

A series of hydroforming experiments using Al-6260-T4 tubes have been performed in a custom hydroforming testing facility developed for this study. The experiments involved inflation of the tubes against a surrounding die, while simultaneously applying axial compression in order to delay wall thinning. Despite this, for some loading paths burst was the limiting failure mode preventing the completion of forming. Numerical simulations revealed a deficiency of the standard quadratic Hill-type anisotropic plasticity in capturing these failures. Independent experiments on the same batch of tubes, involving loading to rupture under combined internal pressure and axial load tracing both radial and corner stress paths (free inflation hydroforming) were undertaken to identify the appropriate constitutive framework for accurate failure predictions. The specimens developed a limit load instability in the form of a pressure maximum, followed by mild axisymmetric bulging at mid-span leading eventually to rupture. Several non-quadratic anisotropic yield functions were scrutinized, with the Barlat *et al.* Yld 2000-2D model exhibiting the best performance for both radial and non-proportional paths. More recently, the calibrated constitutive models have been introduced in numerical simulations of the hydroforming experiments. It will be demonstrated that with the constitutive improvements made, the prediction of localized wall thinning that precipitates burst in hydroforming develops more in concert with the experimentally observed behavior. Thus, the constitutive framework developed enables a more accurate prediction of the tight working envelope of aluminum tube hydroforming.

**Keywords:** Aluminum; Anisotropy; Path-Dependent Failure; Tube Hydroforming

## 1. INTRODUCTION

Tube hydroforming is a manufacturing process that has gained significant popularity in the automotive industry, as well as in other applications [1,2]. It can be used to shape thin-walled structural members of varying cross-section along their length, thus allowing for the structure to be optimized for weight and strength. Aluminum tube hydroforming accentuates this advantage, however is limited by the reduced ductility and by the more complicated constitutive behavior of aluminum alloys in comparison to the steels that are meant to replace.

We present a detailed combined experimental and numerical study of the process for Al-6260-T4 tubes, along with results from an independent but closely linked study of tube formability and of the appropriate constitutive model for that material.

## 2. TUBE HYDROFORMING EXPERIMENTS

A custom facility was designed and constructed to study the hydroforming of relatively long, thin-walled tubes. The facility consists of a hydroforming machine, a pressurizing unit of 20,000 psi capacity and a computerized data acquisition and control system, all custom designed and fabricated for the purposes of this study [3].

### 2.1 Hydroforming facility

We investigate the simple forming operation involving a circular tube that is expanded to the square shape shown in Fig. 1. For a tube of 2.357 in. initial diameter and under ideal forming conditions, this expansion would impart an average hoop strain of about 18%, which is close to the failure strain of Al-6260-T4 in uniaxial tension. The machine is designed to receive tube specimens of 34 in. maximum length. Using 24 in. long dies, the remaining 10 in. can be used for end feeding.

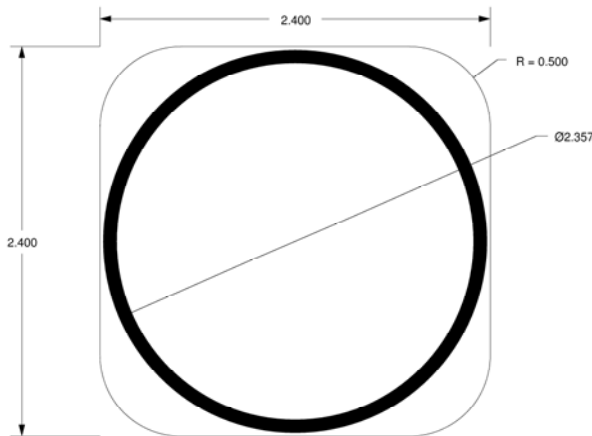


**Figure 1.** Cross-sectional layout of the hydroforming experiment

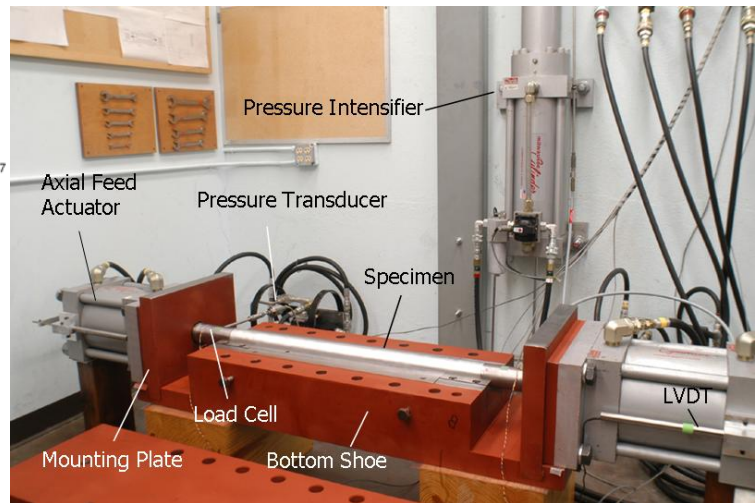


**Figure 2.** Photograph of the hydroforming facility

A picture of the facility is shown in Fig. 2. The body of the machine consists of two steel “shoes” which enclose the forming die and provide support for the axial feed actuators. During forming, the shoes are held together by 14 1.25 in. bolts. The dies are made of P20 tool steel and have overall dimensions of  $24 \times 5 \times 5.05$  in. They were machined with precision ( $\pm 0.002$  in.) and to a surface finish of 63 RMS. The alignment of the dies, including the two shoes, is

facilitated by dowel pins. The required end-feed is provided by two 8 in. bore / 5 in. stroke 150 kip capacity hydraulic actuators, operating on 3,000 psi hydraulic pressure. Pressurization is provided by a 20,000 psi pressure intensifier (“booster”) shown in Fig. 2. The booster also operates on 3,000 psi pressure, while the available volume of high pressure fluid is 0.5 gallons. A compound of 95 parts water / 5 parts Multan 98-10 (Henkel Surface Technologies) is used as the pressurizing fluid.

The whole machine has a footprint of  $94.5 \times 28 \times 24$  in. and weighs approx. 3,250 lbs. Each shoe weighs approx. 1,100 lb without the axial actuator assemblies. The machine is opened and closed using a 1 ton jib crane with a chain hoist.

## 2.2 Data acquisition and control systems

The facility is operated via a six-channel custom system shown schematically in Fig. 3. The same system is used both for feedback control and for data acquisition. It consists of a microprocessor based analog controller, which also provides signal conditioning, and is commanded by custom software running on a PC and created using LabView.

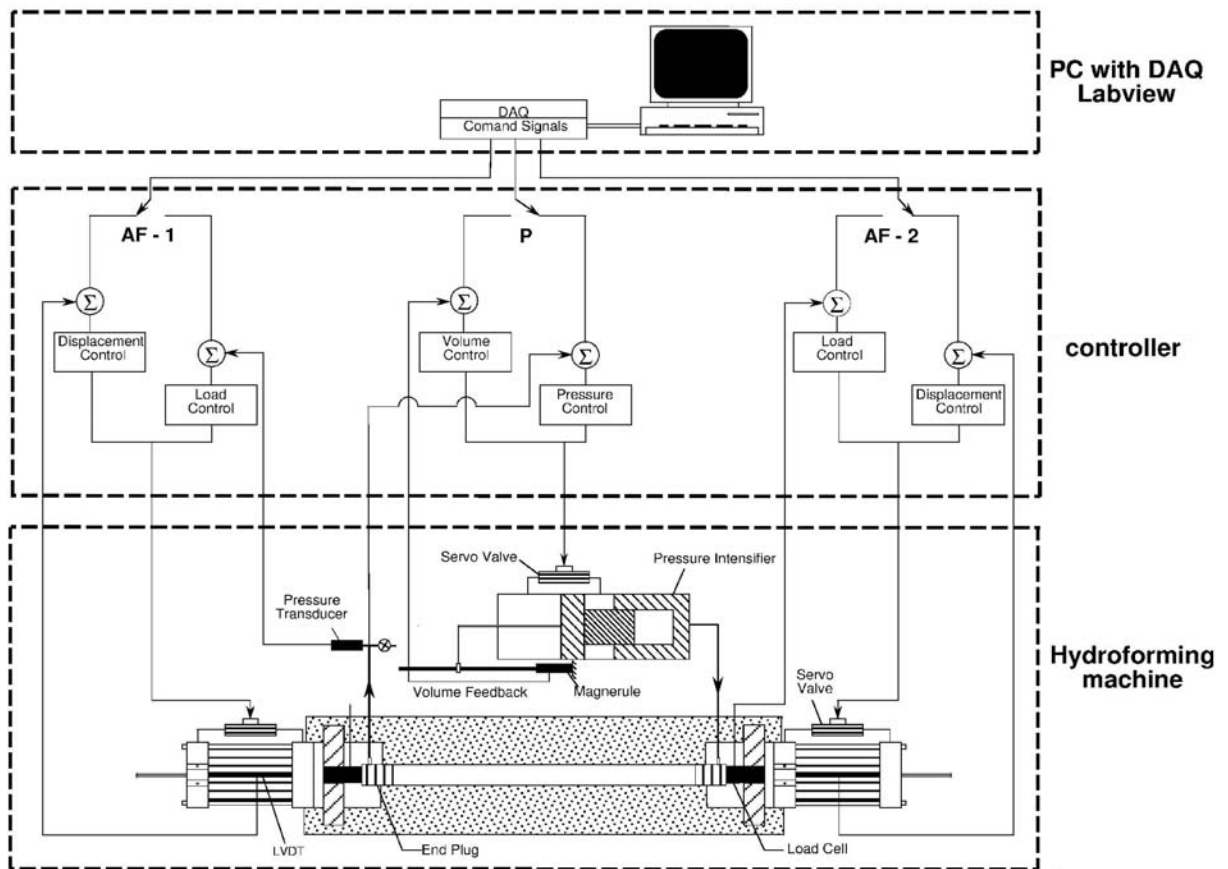


*Figure 3. Data acquisition and control system*

Each axial feed actuator is equipped with a load cell and a displacement transducer. The load cells are custom designed for 150 kips and are positioned between the actuator rams and the specimen. The actuator displacement is monitored using LVDTs with a linear range of  $\pm 3$  in. The pressure is monitored by a 20,000 psi pressure transducer. The volume of the fluid discharged in the specimen is recorded by monitoring the booster tail rod displacement using a

Magnetostrictive Linear Displacement Transducer (MagneRule MRU-3000-018) with a range of 18 in. All sensors were calibrated to the required 10 V standard.

The controller of the facility is based on an extensively modified MTS 458.20 MicroConsole unit and a Personal Computer running a custom Labview application. The MicroConsole has 6 conditioner/controller channels, one for each of the transducers described above. The computer system consists of a PC equipped with two NI PCI-6035E A/D cards. Each card has 8 differential input channels (A/D) with 16-bit resolution and 2 bipolar output channels (D/A) with 12-bit resolution. The maximum sampling rate is 200 kS/s.

The software that is used to acquire the data and to generate the control commands was created in the Labview environment. During the experiment, the software acquires and plots the desired quantities in real-time and also outputs the predetermined command signals. The MTS MicroConsole also performs the feedback control by comparing the output commands from the PC to the system response as monitored by the transducers, issuing the command signals to the three servovalves (Fig. 3). Each function can run under either “displacement” or “load” control. In our experiments, we usually prescribed the axial feed displacements and the internal pressure.

### 2.3 Description of a typical experiment

Each experiment was designed with the help of FE analysis to be described later [4]. Two families of models were employed: fast and efficient 2-D ones and more detailed 3-D models. Given a target cross-sectional shape, the 2-D models were used to establish the required pressure and axial feed and their approximate history. With the benefit of these results, a detailed 3-D calculation was conducted, to establish the final axial feed – internal pressure history.

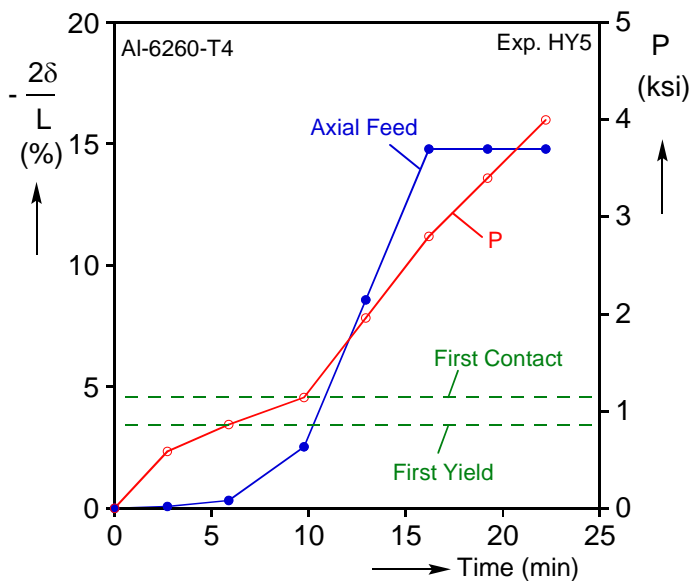


**Figure 4.** Displacement and pressure histories prescribed in the experiment



**Figure 5.** Initial and deformed cross sections of the hydroformed tube (HY8)

A typical loading path is shown in Fig. 4. The axial feed is initially kept low, until the pressure has increased sufficiently to yield the tube and to bring it into contact with the die, averting overall buckling of the long workpiece. After contact, the additional stabilizing effect provided by the die allows for the material to be fed into the forming cavity. Towards the end of the experiment, the axial feed is kept constant while the internal pressure is increased further, to

improve the dimensional accuracy of the final product. In industry the two phases are termed “axial feeding” and “calibration”.

## 2.4 Typical results

The initial and deformed cross-sections of a tube are shown in Fig. 5. Burst was a major limiting factor in our experiments. Since burst is associated with wall-thinning, of interest is the circumferential thickness distribution in the final product shown in this figure.

Because of the relatively long specimens formed, and despite the tubes being lubricated (Henkel PTD-1424 BX), friction restricted the material flow in the forming cavity. This for example is quantified in Fig. 6, which shows the variation of compressive strain along the formed tube. The friction in turn reduced the effect that axial feeding can have in delaying burst.

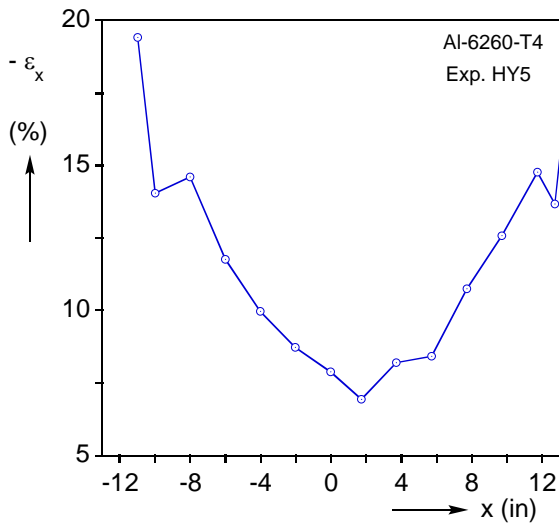


**Figure 6.** Axial strain distribution in the tube after hydroforming

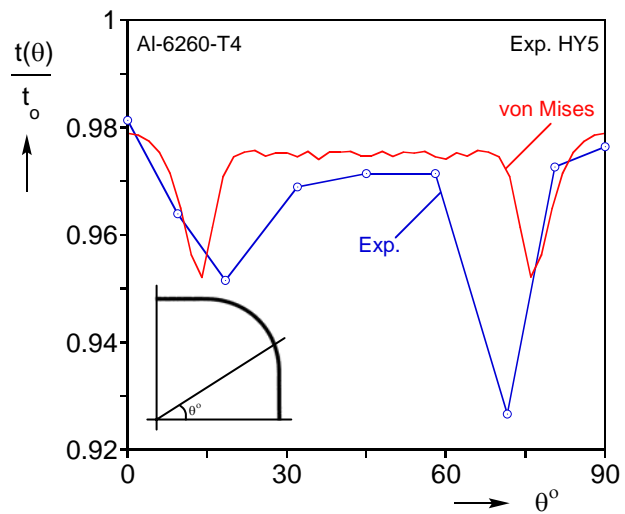


**Figure 7.** Circumferential thickness distribution at mid-span and prediction using von Mises.

The circumferential thickness variation for a quadrant of a formed tube at mid span is given in Fig. 7. It can be noted that the maximum reduction in thickness occurs at the intersection of the flat and the curved sides of the cross section. This pattern consistently occurred in all of our experiments. It can be attributed to friction, since any part of the cross section that contacts the die is restrained in its further movement along the circumference. It was observed that such deep grooves tend to lead into fracture failure at higher pressures.

Included in Fig. 7 is the prediction of thickness using the von Mises yield function. The average thickness of the final product is reproduced quite well. However, the localized thinning which precipitates burst is not captured. We found this to be a direct consequence of the use of a quadratic yield function, which is well known to be unsuitable for aluminum alloys. Hence a separate study on Al tube formability, aiming at arriving at a constitutive framework suitable for the prediction of burst was undertaken [5,6,11] and is outlined next.

## 3. TUBE FORMABILITY

### 3.1 Experimental facility

Tubes from the same batch were first loaded under internal pressure and axial load along radial paths in the stress space and taken to failure (free inflation) [5]. The experiments were

performed on a standard servohydraulic testing machine coupled to an independent pressurizing unit (see Fig. 1 in [5]). Each specimen was equipped with strain gages and axial and circumferential extensometers. In addition, a square grid of lines was slightly scribed on the surface of the specimens, to acquire the local strains around the zone of failure.

To trace the radial paths, the tubes were inflated under volume control; a pressure transducer was monitoring the induced pressure in the specimen; and the servohydraulic machine was running under load control, with the load set to remain at a fixed ratio to the induced pressure. Thus, the experiments were performed under constant load/pressure ratios, therefore tracing radial paths in the stress space.

### 3.2 Radial experiments

A summary of the radial path experiments is given in Fig. 8, while four of the tested specimens are shown in Fig. 9. During the inflation, the specimen deformed uniformly (except at the ends where it is clamped) until a limit load instability, in the form of a pressure maximum, developed. Since the tubes were inflated under volume control, the experiment could continue past that instability. Soon after the pressure maximum, a mild axisymmetric bulge appeared at mid-span. Depending on the particular path, the deformation could continue well past the pressure maximum. At some point and under decreasing pressure, the axisymmetric bulge evolved suddenly into a non-axisymmetric one, the deformation localized rapidly and the specimen burst dynamically. However, as a result of the way the experiments were performed, it was possible to arrest the failures as evident from Fig. 9. The left-most specimen in the figure shows clearly the axisymmetric bulge that developed during the deformation while the right-most specimen failed around the circumference as the axial stress is dominant for  $\alpha \geq 1$ .

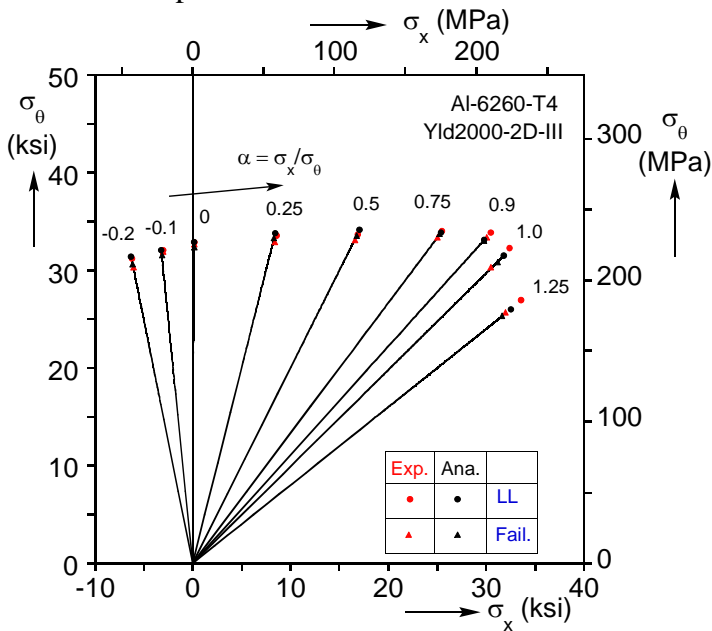


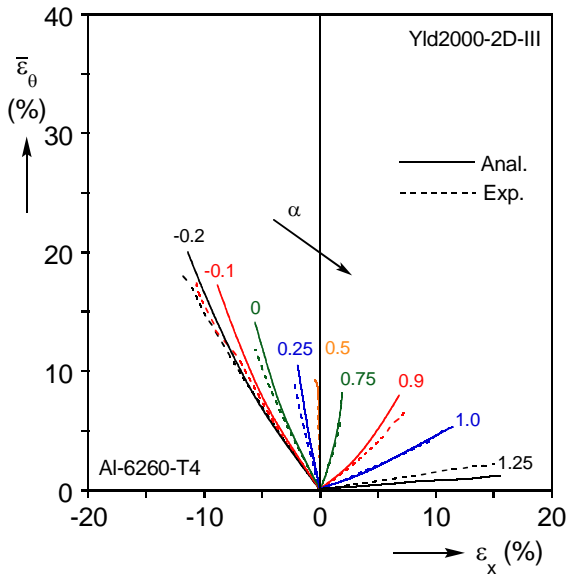
Figure 8. Stress paths in the radial experiments and predictions using the Yld2000-2D model.



Figure 9. A set of failed test specimens tested at different biaxiality ratios: from left to right  $a = -0.2, 0, 0.75, 1.0$ .

The strain paths that correspond to the radial stress paths, shown in Fig. 10, are almost linear as well (truncated at the maximum pressure). The average strains at the onset of failure, as measured by the extensometers, are given in Fig. 11. Depending on the path, they can be significantly different from those at the maximum pressure. The local strain measurements

performed post-mortem with the aid of the strain grid are not included here, but they are approximately twice as large as the extensometer recordings (see [5]), indicating the localization of plastic deformation prior to the failure.



**Figure 10.** Comparison of calculated and measured engineering strain paths for radial loading paths, using the Yld2000-2D yield function.

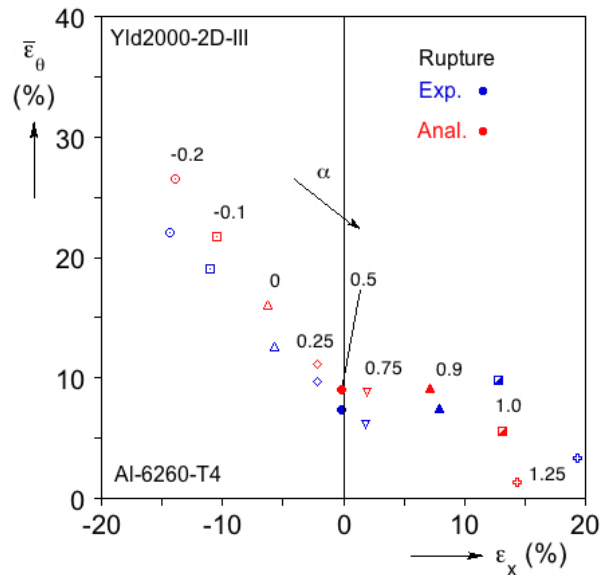


**Figure 11.** Comparison of measured and calculated average strains at rupture using the Yld2000-2D yield function.

## 4. NUMERICAL AND CONSTITUTIVE MODELING OF FREE INFLATION

### 4.1 Yield functions

The main objective of the free inflation experiments was to establish the appropriate constitutive framework for accurate predictions of burst. Initially the von Mises and quadratic anisotropic Hill models were examined, which failed to yield accurate predictions of the strain paths. More advanced non-quadratic yield functions were subsequently employed [5,6], including those of Hosford (isotropic and anisotropic versions), Karafillis and Boyce, and Barlat *et al.* [7-10]. In the order presented, these offer increased flexibility in reproducing the experimental yield loci. The trade-off however is that the calibration becomes more elaborate. In fact, for the best performing model (Barlat *et al.* Yld 2000-2D) to provide accurate predictions of failure, an elaborate calibration procedure had to be employed [6].

### 4.2 Finite element modeling

The free inflation experiments were simulated in Abaqus/Standard. The various yield functions were implemented in User Material Subroutines (UMATs) using an associated flow rule and isotropic hardening [5,6]. Two distinct FE models were developed, to capture the two modes of failure observed experimentally. In each case, the tube was modeled as a perfect cylinder equipped with a suitably oriented groove of reduced thickness, as in an M-K analysis. The models were meshed with shell elements with reduced integration and are inflated with the aid of hydrostatic elements. Riks' path-following method is used to allow tracking the response past the maximum pressure. The numerical models reproduce quite faithfully the events observed in the free inflation experiments. The quantitative agreement however is strongly

dependent on the constitutive model employed, especially for the failure strain predictions. The results from the best performing model are included in Figs. 8, 10 and 11, which show excellent agreement for the stress and strain paths and for the stresses at the maximum pressure and at the onset of failure. The agreement of the calculated strains at the onset of failure to the experimental results is quite good, as well.

### 4.3 Corner paths

The tube formability study was concluded by examining the effect of the loading path on failure [11]. A series of corner path tests, each associated with a corresponding radial path, were performed. Although such paths are rather extreme cases, they represent the loading encountered in an actual hydroforming operation more faithfully than the radial paths do. In these experiments, the strains at the onset of failure are distinctly path dependent, as expected. However, it was discovered that the failure stresses also exhibit path dependence, especially as the prestrain increases. A possible explanation is that for the specific aluminum alloy studied, the evolution of the yield surface is dominated by isotropic hardening (see [11]).

## 5. TUBE HYDROFORMING SIMULATIONS

The hydroforming experiments were simulated using Abaqus/Standard. Models of different degrees of complexity were developed and are outlined below (see also [4]).

### 5.1 Generalized plane strain model (2-D)

The simplest model for tube hydroforming is limited to the plane of the cross section, but includes a uniform normal displacement or load, associated with the axial feed. Exploiting the symmetries of the geometry, only one quarter of the tube at mid-span is examined. After suitable parametric studies, a mesh of  $4 \times 98$  (thickness  $\times$  hoop) linear elements with reduced integration was selected. The use of linear elements was dictated by the presence of contact.

Such 2-D models afford very fast runs that can be very useful in the preliminary design of a hydroforming experiment. They reproduce quite well both the shape and the average thickness of the tube at mid-span (Fig. 7). However, they fail to capture the localization that precedes bursting. Further, since the axial strain varies along the tube length (Fig. 6), the actual axial feed at mid-span is not known a priori. Thus, in the context of this work they have been used only to provide initial guesses of the loading conditions (pressure and axial feed) and of their histories.

### 5.2 3-D model with shell elements

The simplest 3-D model of hydroforming employs shell elements. Only  $1/8^{\text{th}}$  of the actual tube needs to be considered (Fig. 12). The tube is meshed with linear shell elements with reduced integration, arranged as  $40 \times 77$  (circumference  $\times$  length). The elements have 7 through-thickness integration points and Simpson's rule is used.

Included in Fig. 12 is the deformed configuration, which clearly shows the axial variation of the shape of the formed tube caused by friction. By comparing the experimental finding (Fig. 6) with the numerical predictions, it is found that  $\mu = 0.2$  is the most appropriate Coulomb friction coefficient. A close-up at mid-span is shown in Fig. 13, where the thickness reduction is observed to localize at the same spots as in the experiments. Such predictions from the various constitutive models employed are plotted in Fig. 14, along with the experiment. It can be seen from Fig. 14a that the different constitutive models yield similar predictions. This is somewhat surprising, since in the free inflation case the details of each model were quite decisive in the

accuracy of the bursting predictions [5,6]. On the contrary, it appears that the predictions are quite sensitive to the exponent of the yield function (Fig. 14b), even though the exponent that matches the thickness reduction best, does not predict the average thickness of the final tube accurately. In addition, the specific exponent has been selected arbitrarily to match that experiment. In an effort to resolve these questions, FE models using solid elements are developed in the following section.

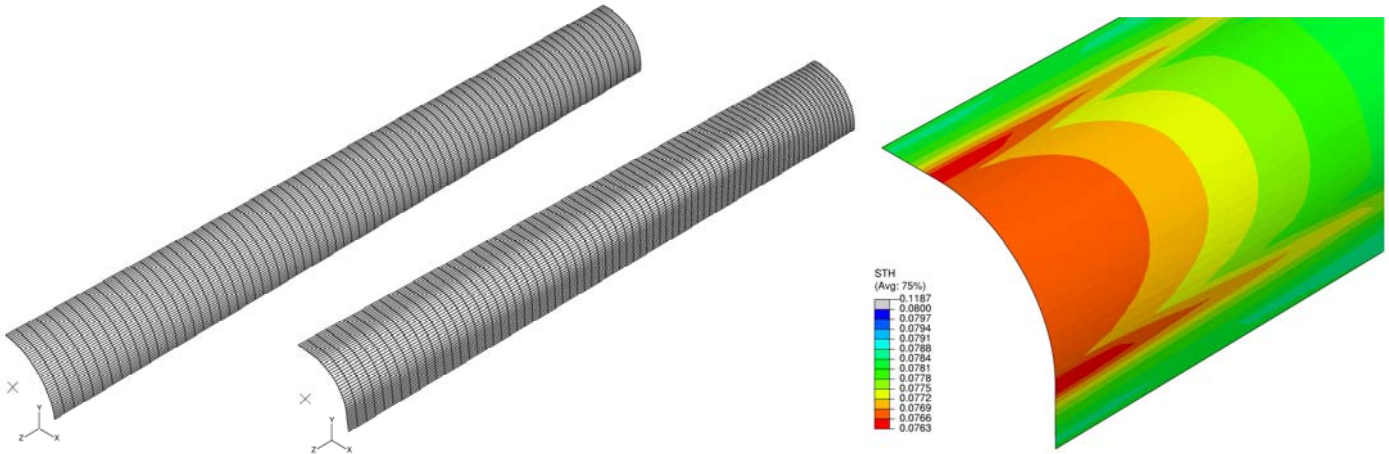


**Figure 12.** Original and deformed configurations of the shell element model (die removed for clarity)

**Figure 13.** Thickness contours at midspan

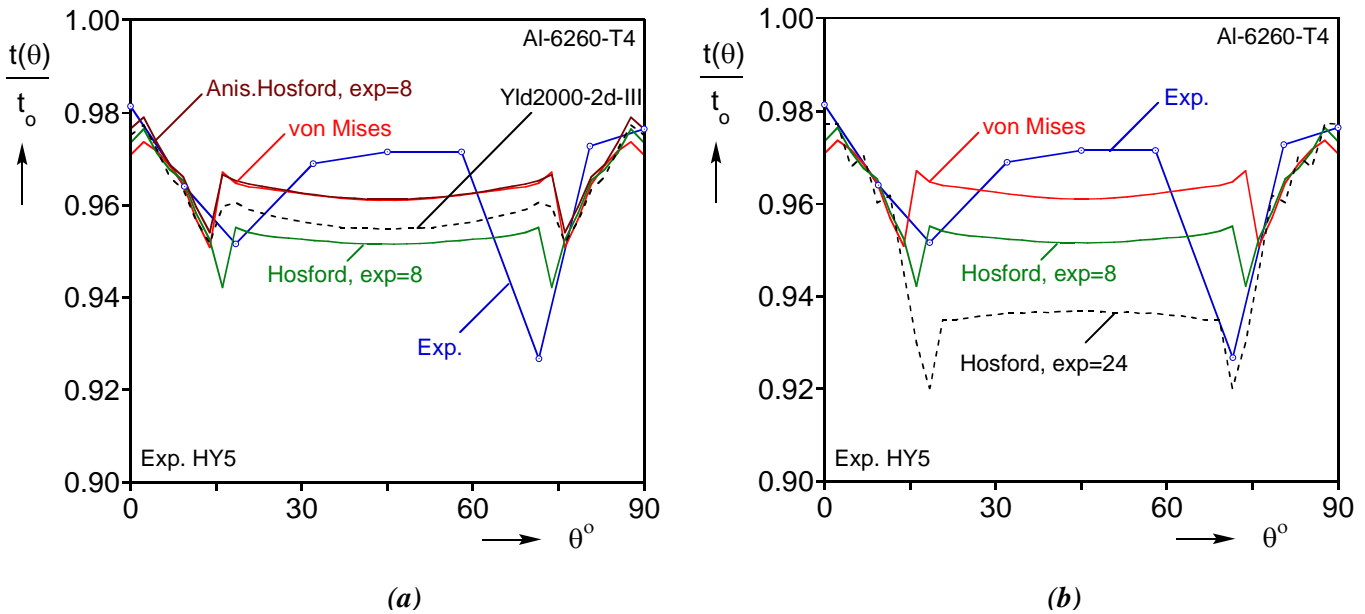


**Figure 14.** Circumferential thickness distribution at mid-span. Effect of (a) anisotropy, and (b) exponent.

**5.3 3-D model with solid elements**

In FE simulations of sheet metal forming processes, shell elements are preferred because of the thin-walled geometries involved and the efficiency that they offer. However, in problems such as the present one in which localized wall thinning develops, coupled with normal stresses

due to contact one side and pressure on the other, the stress triaxiality should not be neglected. To address this, a fully 3-D model meshed with solid elements was developed.

The model is again representing  $1/8^{\text{th}}$  of the actual tube and is meshed with linear continuum elements arranged as  $60 \times 3 \times 45$  (circumference  $\times$  thickness  $\times$  length). This model also captures the axial variations observed experimentally, but in addition, allows for more realistic predictions of thickness reduction. Shown in Fig. 15 are deformed configurations at mid-span of tubes modeled with the von Mises and the non-quadratic Hosford yield functions at the same point in the loading history. In the second model, the localization of wall thinning is much more significant. This difference is more clearly quantified in the plot shown in Fig. 15c. It can be concluded then that for accurate predictions of failure in Al tube hydroforming, non-quadratic yield functions combined with solid elements need to be used. The inclusion of anisotropy in the non-quadratic models may accentuate this difference further.

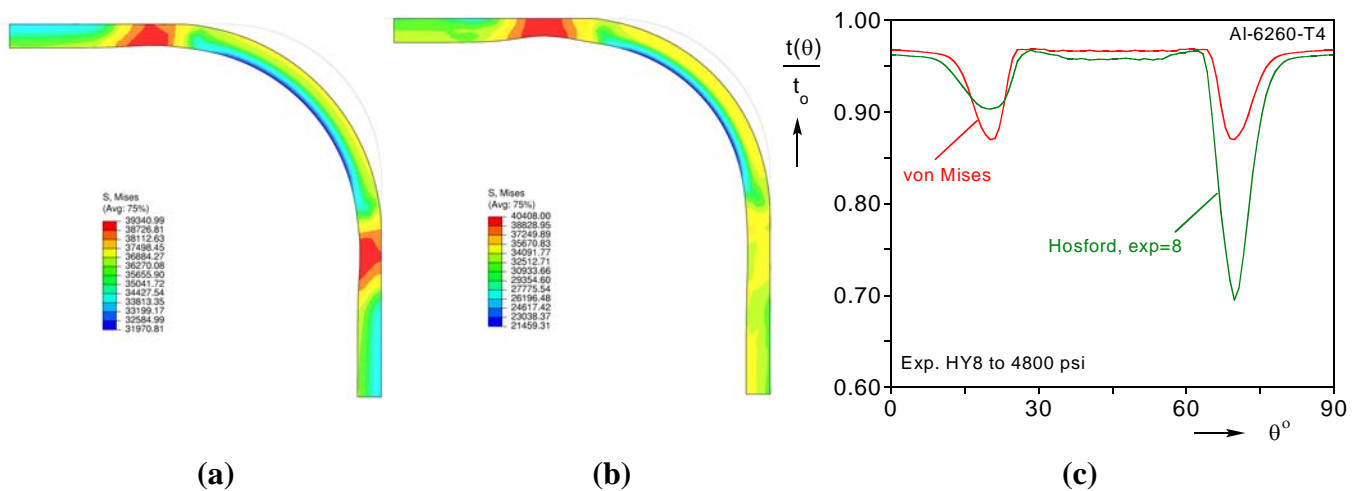


**Figure 15.** Deformed configurations from solid element model at midspan, with (a) von Mises and (b) Isotropic Hosford ( $exp=8$ ) models. (c) Circumferential thickness distribution at mid-span

## 6. CONCLUSIONS

The paper summarizes results from a broad study of hydroforming of Al-6260-T4 tubes that includes an investigation on the formability of this material and the best ways to model its constitutive behavior. The approach involves a combination of experiments and analysis.

A custom tube hydroforming facility and experiments performed with it were described. During forming, bursting was a major limiting factor. In order to predict this mode of failure satisfactorily, an independent study of tube formability was undertaken, where the tubes were tested to failure under radial and corner paths (free inflation) in the axial-hoop stress space. The radial paths were used to calibrate suitable anisotropic yield functions for bursting predictions. These were subsequently tested using corner stress paths. These tests revealed that the failure strains are distinctly path-dependent, as expected, but also that the failure stresses can be path-dependent as well, especially as the prestrain increases.

As is well established in the literature, aluminum alloys require the use of a non-quadratic yield functions. Indeed, use of properly calibrated Yld2000-2D with exponent 8 lead to good prediction of failure stresses, strain paths and failure strains. The same yield function yielded reasonably good predictions of failure in the corner paths.

The constitutive models developed were subsequently implemented in numerical simulations

of the hydroforming experiments performed, using both shell and solid elements. In both cases, use of non-quadratic yield functions improves the prediction of localized wall thinning that precipitates failure. However, solid elements were found to be significantly more effective in capturing this type of localization because they can better reproduce the local stress triaxiality.

## 7. ACKNOWLEDGEMENTS

The authors acknowledge with thanks financial support of this work received from the National Science Foundation through Grant DMI-0140599 and supplementary funding provided by G.M. with Robin Stevenson as coordinator. Special thanks to Alcoa and Edmund Chu for providing initial seed funding for the project and the tubes analyzed and tested. Discussions with Frederic Barlat were instrumental in the adoption of the Yld2000-2D yield function.

## 8. REFERENCES

1. H. Singh, "Fundamentals of hydroforming", 2003, SME, Dearborn , MI
2. M. Koc (Ed.) "Hydroforming for advanced manufacturing", 2008, Woodhead Publ. & CRC Press, Boca Raton, FL
3. Y.P. Korkolis and S. Kyriakides, "Hydroforming of anisotropic aluminum tubes. Part I: experiments", (*in preparation*)
4. Y.P. Korkolis and S. Kyriakides, "Hydroforming of anisotropic aluminum tubes. Part II: analysis", (*in preparation*)
5. Y.P. Korkolis and S. Kyriakides, "Inflation and burst of anisotropic aluminum tubes for hydroforming applications", *Int'l J. Plasticity*, 24/3 (2008) 509-543
6. Y.P. Korkolis and S. Kyriakides, "Inflation and burst of anisotropic aluminum tubes, part II: an advanced yield function including deformation-induced anisotropy", *Int'l J. Plasticity*, 24/9 (2008) 1625-1637
7. W.F. Hosford, "A generalized isotropic yield criterion". *ASME J. Appl. Mech.* 309 (1972), 607-609.
8. W.F. Hosford, "On yield loci of anisotropic cubic metals". Proc. 7th NAMRC, (1979), SME, Dearborn, MI, 191-196.
9. A.P. Karafillis, A.P. and M.C. Boyce. "A general anisotropic yield criterion using bounds and a transformation weighting tensor". *J. Mech. Phys. Sol.* 41, (1993), 1859-1886.
10. F. Barlat, J.C. Brem, J.W. Yoon, K. Chung, R.E. Dick, D.J. Lege, F. Pourboghrat, S.-H. Choi, and E. Chu. "Plane stress function for aluminum alloy sheets-part I: theory". *Int'l J. Plasticity* 19, (2003), 1297-1319.
11. Y.P. Korkolis and S. Kyriakides, "Path-dependent failure of inflated aluminum tubes", *Int'l J. Plasticity*, (in press, doi:10.1016/j.ijplas.2008.12.016)